

# Low-Dose CT Reconstruction Using Dataset-free Learning

Feng Wang<sup>a</sup>, Renfang Wang<sup>a,\*</sup>, Bo Yang<sup>b</sup> and Hong Qiu<sup>a</sup>

<sup>a</sup>College of Big Data and Software Engineering, Zhejiang Wanli University, Ningbo, 315100, Zhejiang, China

<sup>b</sup>Key Laboratory of Geoscience Big Data and Deep Resource of Zhejiang Province, School of Earth Sciences, Zhejiang University, Hangzhou, 310027, Zhejiang, China

## ARTICLE INFO

**Keywords:**  
X-ray CT  
Low-dose CT  
Deep learning  
Training data-free learning

## ABSTRACT

Low-Dose computer tomography (LDCT) is an ideal alternative to reduce radiation risk in clinical applications. Although supervised-deep-learning-based reconstruction methods have demonstrated superior performance compared to conventional model-driven reconstruction algorithms, they require collecting massive pairs of low-dose and norm-dose CT images for neural network training, which limits their practical application in LDCT imaging. In this paper, we propose an unsupervised and training data-free learning reconstruction method for LDCT imaging that avoids the requirement for training data. The proposed method is a post-processing technique that aims to enhance the initial low-quality reconstruction results, and it reconstructs the high-quality images by neural network training that minimizes the  $\ell_1$ -norm distance between the CT measurements and their corresponding simulated sinogram data, as well as the total variation (TV) value of the reconstructed image. Moreover, the proposed method does not require to set the weights for both the data fidelity term and the plenty term. Experimental results on the AAPM challenge data and LoDoPab-CT data demonstrate that the proposed method is able to effectively suppress the noise and preserve the tiny structures. And these results also show the proposed method's low computational cost and rapid convergence. The source code is available at <https://github.com/linfengyu77/IRLDCT>.

## 1. Introduction

X-ray computed tomography (CT) is an essential imaging modality for clinical purposes, as it provides high-resolution images of the internal structure of the human body. However, X-ray radiation is known to be harmful to healthy tissues. In some major clinical tasks, a single CT scan can expose patients to radiation doses of up to 43 mSv Smith-Bindman, Lipson, Marcus, Kim, Mahesh, Gould, Berrington de González and Miglioretti (2009), which may increase the risk of cancer. Consequently, reducing radiation dose while obtaining high-resolution images has become a significant area of research in CT scanning.

Currently, there are two primary strategies for reducing CT radiation dose: (1) decreasing the number of projection views and (2) lowering the X-ray tube current. This approach is commonly referred to as LDCT. LDCT algorithms can be broadly categorized into four groups: sinogram domain filtering, iterative reconstruction, and deep learning-based reconstruction.

Sinogram domain filtering methods exploit the distinct distributions of desired signals and noise in the sinogram domain to reconstruct CT images. This technique involves filtering out components corresponding to artifacts or noise in the sinogram domain and then inverting the filtered sinogram data into the image domain using analytic algorithms. Numerous analytic filtering methods have been proposed based on the distribution of noise. For instance, filtered back projection (FBP) is a classical reconstruction method for CT images that performs high-pass filtering in the sinogram

domain before back-projection. Sinogram domain filtering can produce high-quality CT images when the noise distribution is accurately characterized. However, determining this distribution can be challenging, particularly since artifacts or noise often correlate with image structures.

Compared with sinogram domain filtering methods, iterative reconstruction approaches are more flexible and stable. Iterative reconstruction approaches can be further divided into hybrid iterative reconstruction methods and model-based iterative reconstruction methods. Hybrid iterative reconstruction method produces an image by adjusting the statistical characters of the sinogram domain and the image domain. Model-based iterative reconstruction method utilizes the process of alternately performing the forward-projection (i.e., sinogram data generation) and back-projection (i.e., CT image reconstruction) to achieve iterative filtering in the sinogram domain and the image domain. Furthermore, the cost function of model-based iterative reconstruction method usually consists of a fidelity term with the noise model in the sinogram domain and a regularization term with the prior model in the image domain. The regularization term plays a vital role in reconstruction, and many regularizations have been proposed, such as total variation (TV) Sidky and Pan (2008); Kim, Ye, Worstell, Ouyang, Rakvongthai, Fakhri and Li (2015), low-rank Cai, Jia, Gao, Jiang, Shen and Zhao (2014), non-local means (NLM) Ma, Zhang, Gao, Huang, Liang, Feng and Chen (2012); Zhang, Xi, Yang, Cong, Zhou and Wang (2016), and dictionary learning Qiong Xu, Hengyong Yu, Xuanqin Mou, Lei Zhang, Jiang Hsieh and Ge Wang (2012). The model-based iterative reconstruction method usually has better performance than hybrid iterative reconstruction method, but it is also computationally expensive. Additionally, model-based iterative reconstruction method requires

\*Corresponding author

 wangf\_721@zju.edu.cn ( Feng Wang); renfang\_wang@126.com ( Renfang Wang); bo.yang@zju.edu.cn ( Bo Yang); qiuHong@zju.edu.cn ( Hong Qiu)

ORCID(s): 0000-0002-8717-8893 ( Feng Wang)

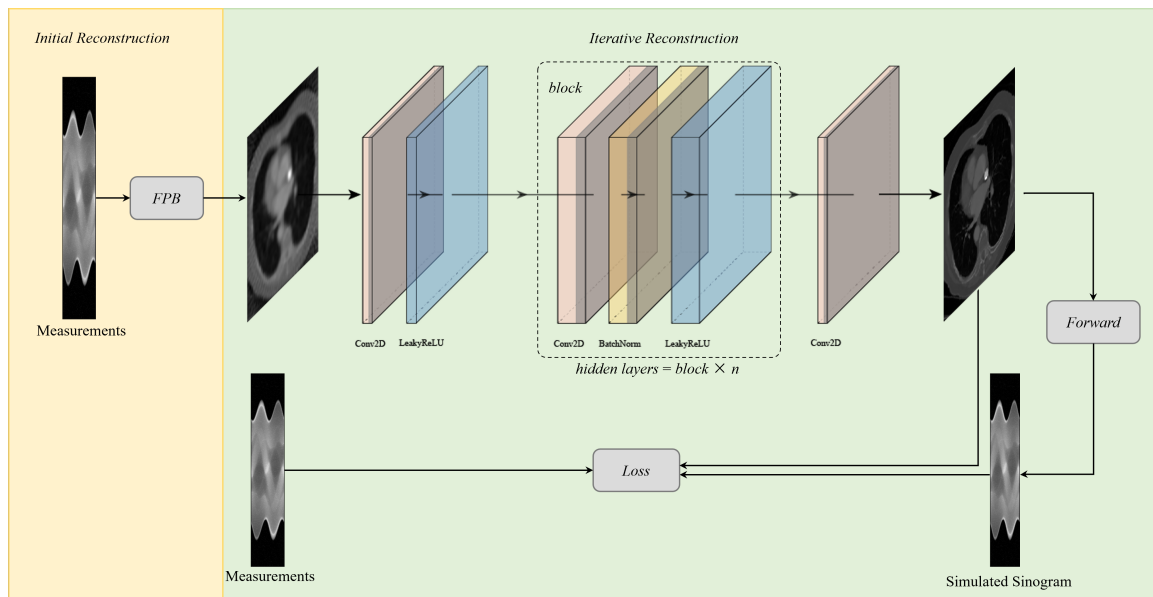


Figure 1: Schematic diagram of the proposed method.

manually designing the proper regularization and choosing the weight to obtain satisfactory reconstruction results.

In recent years, deep learning techniques have been employed in LDCT reconstruction, and they have demonstrated better performance than conventional LDCT reconstruction methods. Deep learning-based LDCT reconstruction methods can be categorized into four groups: sinogram domain processing (SDP), image domain processing (IDP), dual-domain processing (DDP), sinogram-image direct mapping (SIDP), and model-based deep learning (MBDL).

The SDP reconstruction algorithm aims to use a pre-trained neural network to inpaint the LDCT measurements into sinogram data that is very close to normal-dose CT (NDCT) measurements. For instance, Yuan, Zhou, Gong and Qi (2019) proposed a sinogram domain denoising approach using a convolutional neural network (CNN) with a filter loss function. Compared with image domain denoising methods, these approaches can easily estimate the noise level in the projection. Reference Liu and Li (2020) proposed a sinogram data interpolation method by leveraging a conditional adversarial network (GAN). Although sinogram domain processing can correct errors in the sinogram domain, errors produced by the shortcomings of conventional methods can still negatively affect the final reconstructions.

In contrast to the SDP algorithm, IDP produces high-quality CT images by using a neural network to denoise the initial reconstructed images with artifacts. Most deep learning methods employ IDP to improve the quality of reconstructed images obtained using existing methods such as FBP Jin, McCann, Froustey and Unser (2017); Chen, Zhang, Kalra, Lin, Chen, Liao, Zhou and Wang (2017). IDP is more straightforward compared to the SDP algorithm. However, one main disadvantage of SDP is that it is difficult to recover information lost from the initial reconstructed images, which serve as inputs to the neural network.

DDP is a method that combines SDP and IDP. It leverages the advantages of both SDP and IDP to achieve higher-quality images compared to single-domain processing reconstruction methods. Reference Kang, Min and Ye (2017) combined a deep convolutional neural network (CNN) with directional wavelet transform to extract the directional component of artifacts in low-dose CT images and exploit intra- and inter-band correlations. Reference Zheng, Gao, Zhang and Xing (2020) proposed a deep learning-based function optimization method for LDCT imaging, which incorporated the Radon inverse operator and disentangled each slice. Although DDP can achieve good inversion results, it requires a larger training dataset due to its two training procedures: sinogram domain and image domain.

SIDP is an end-to-end reconstruction algorithm that directly transforms sinogram data into CT images. This method has the lowest complexity as it only requires training a neural network without extra processing such as sinogram data correction and inversion. For example, Zhu, Liu, Cauley, Rosen and Rosen (2018) presented a unified framework for image reconstruction called Automated Transform by Manifold Approximation (AUTOMAP), which directly converts sinogram data into CT images. Reference Kandarpa, Bousse, Benoit and Visvikis (2021) proposed a direct reconstruction framework exclusively using deep learning architectures, which consists of denoising, reconstruction, and super resolution (SR). SIDP is a highly efficient reconstruction method but demands massive memory as the entire sinogram data needs to be fed into the neural network.

MBDL, also known as optimization unrolling scheme or plug-and-play, is an effective approach that replaces the parameters or regularization of conventional iterative schemes with learnable/pre-trained neural networks. Reference Wu, Kim and Li (2019) unrolled the proximal gradient descent

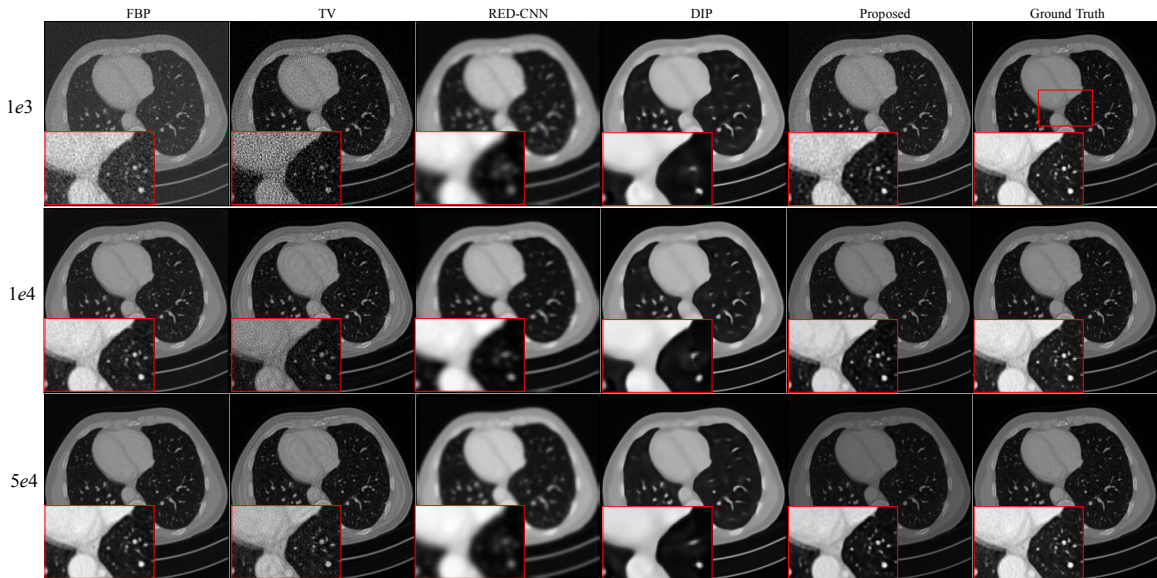


**Figure 2:** Reconstruction results of case AAPM-1 at different dose levels by different methods. Zoomed parts over the region of interest (ROI) marked by the red box in the ground-truth image.

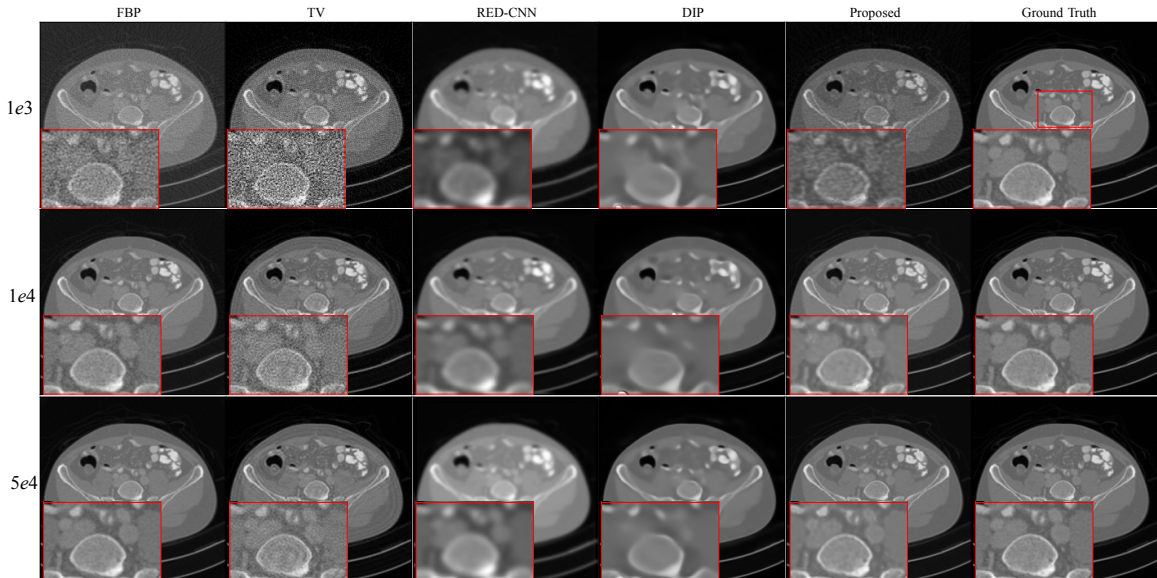


**Figure 3:** Reconstruction results of case AAPM-2 at different dose levels by different methods. Zoomed ROI images from the ground-truth image.

algorithm for iterative image reconstruction to finite iterations and replaced terms related to the penalty function with trainable CNN to reduce memory requirements and training time. Reference Cheng, Wang, Li and Duan (2020) incorporated the benefits from analytical reconstruction methods, iterative reconstruction methods, and DNNs. They unrolled proximal forward-backward splitting into iterative reconstruction updates of CT data fidelity and DNN regularization with residual learning. By leveraging the advantages of deep learning and conventional methods, MBDL offers better interpretability than data-driven deep learning.

Recently, dataset-free methods have drawn much attention in LDCT imaging. These methods can avoid the need for

real data such as high-dose CT images and the sinogram data of high-dose CT images used in supervised deep learning. One unsupervised approach is to denoise the reconstructed CT images using a neural network trained on image pairs with random noise. Reference Yuan, Zhou and Qi (2020) and Hasan, Mohebbian, Wahid and Babyn (2021) employed a denoising network called Noise2Noise Lehtinen, Munkberg, Hasselgren, Laine, Karras, Aittala and Aila (2018) trained on image pairs with independent noise, followed by removing artifacts from the reconstructed LDCT images. Reference Hendriksen, Pelt and Batenburg (2020) trained a Noise2Self Batson and Royer (2019) to solve the tomography problem by modeling the artifacts of LDCT images as

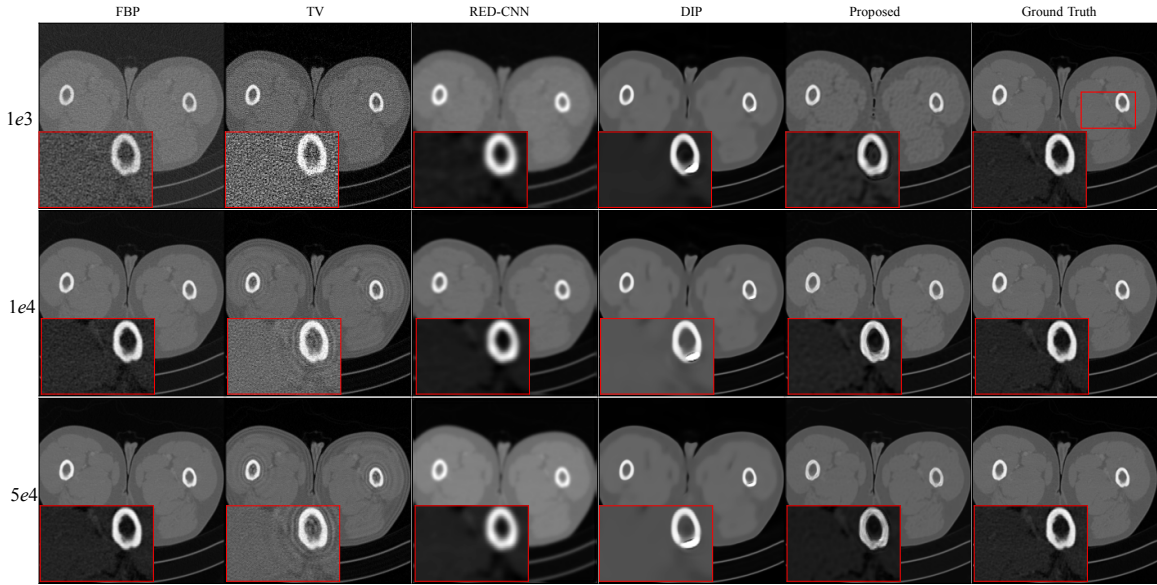


**Figure 4:** Reconstruction results of case AAPM-3 at different dose levels by different methods. Zoomed ROI images from the ground-truth image.

independent random noise. However, these methods suffer from an assumption that simplifies the artifacts, which are highly correlated to the entries of CT images, as random noise.

Another type of unsupervised reconstruction method is built on the consistency between CT measurements and sinogram data modeled on the reconstructed image. For instance, the deep image prior (DIP) Ulyanov, Vedaldi and Lempitsky (2020), originally proposed for natural image denoising by using early stopping to fit the noisy image, has been widely exploited in medical imaging Gong, Catana, Qi and Li (2019); Yokota, Kawai, Sakata, Kimura and Hontani (2019); Yoo, Jin, Gupta, Yerly, Stuber and Unser (2021). Similar to the first unsupervised approach, DIP treats noise as i.i.d random noise rather than artifacts correlated to the entries of CT images. Reference Ding, Ji, Quan and Zhang (2022) proposed an unsupervised LDCT reconstruction method based on Bayesian inference, which takes the  $\mathcal{J}$ -invariant transform of the FBP reconstructed image as the initial value. This method can reconstruct high-quality images from measurements; however, its reconstruction time is significantly higher than that of its competitors.

In this paper, we propose an iterative LDCT reconstruction method that utilizes neural network to improve the CT images reconstructed by FBP method without training data. During the iterative LDCT reconstruction, we minimize the loss, which consists of two components: the  $\ell_1$ -norm distance between the CT measurements and the sinogram data modeled on the post-processed image, and the TV value of the post-processed image. We achieve this by training a neural network. The proposed method does not require collecting any training data and balancing the contribution of data fidelity and TV regularization in the loss. Once the network training is complete, the high-quality reconstructed results will be output immediately.

The rest of the paper is organized as follows: Section II describes how to build and solve the optimization problem. Section III presents the experimental setup and results using the 2016 Low-dose CT Grand Challenge data and the LoDoPaB-CT data Leuschner, Schmidt, Baguer and Maass (2021a). Section IV is the discussion and conclusion.

## 2. Methodology

In this section, we introduce a proposed method for reconstructing LDCT from noisy measurements. This method utilizes a DNN to enhance the CT image reconstructed by the FBP method, without the need for training data.

### 2.1. Problem Setup

The forward formulation of LDCT can be formulated as,

$$\mathbf{y} = \mathbf{Ax} + \epsilon, \quad (1)$$

where  $\mathbf{y}$  represents the CT measurements,  $\mathbf{A}$  is the projection matrix of CT imaging,  $\epsilon$  denotes the background contributions of scatter and electrical noise, and  $\mathbf{x}$  represents the ground-truth CT image. Typically, we can solve the inverse problem of Eq. 1 by using the FBP method,

$$\mathbf{x}_{fbp} = \mathcal{F}(\mathbf{y}), \quad (2)$$

where  $\mathbf{x}_{fbp}$  is the reconstructed image by FBP. However, due to the low source intensity of X-ray and/or the random noise, the quality of  $\mathbf{x}_{fbp}$  is unsatisfactory, often suffering from noticeable streaky artifacts, random patterns, and low resolution.

Considering a DNN  $\mathcal{NN}$  with parameters  $\theta$  that can enhance the image's quality by  $\hat{\mathbf{x}} = \mathcal{NN}(\mathbf{x}_{fbp}; \theta)$ . We can

establish the maximum a posterior (MAP) estimator for the desired high-quality CT image  $\mathbf{x}^*$  as,

$$\mathbf{x} \simeq \mathbf{x}^* = \arg \max_{\hat{\mathbf{x}}} p(\mathbf{x} | \hat{\mathbf{x}}). \quad (3)$$

Furthermore, according to Bayesian theorem, the posterior distribution  $p(\mathbf{x} | \hat{\mathbf{x}})$  of the ground-truth  $\mathbf{x}$  given  $\hat{\mathbf{x}}$  can be formulated as,

$$p(\mathbf{x} | \hat{\mathbf{x}}) = p(\hat{\mathbf{x}} | \mathbf{x})p(\mathbf{x})/p(\hat{\mathbf{x}}). \quad (4)$$

To solve the optimization problem of Eq. 3, many existing LDCT reconstruction algorithms tend to set up the likelihood term  $p(\mathbf{x}^* | \mathbf{x})$  with the assumption of independent and identically normally distributed Gaussian noise  $\epsilon \sim \mathcal{N}(0, \sigma^2 I)$ ,

$$p(\hat{\mathbf{x}} | \mathbf{x}) = \frac{1}{2\sigma^2} \|\mathbf{y} - \mathbf{A}\hat{\mathbf{x}}\|_2^2. \quad (5)$$

However, the artifacts in LDCT images are highly correlated to the entries of CT images rather than random noise. Moreover, the results inverted through  $\ell_2$ -norm loss tend to be over-smoothed, which is not beneficial for preserving the tiny structures and/or sharp edges. Hence, we propose to replace the  $\ell_2$ -norm with  $\ell_1$ -norm, we then obtain the MAP object for  $\theta^*$ ,

$$\theta^* = \arg \min_{\theta} \|\mathbf{y} - \mathbf{A}\hat{\mathbf{x}}\|_1. \quad (6)$$

Furthermore, we add the TV term of the reconstructed CT image  $\hat{\mathbf{x}}$  into Eq. 6 as a smooth penalty to overcome the potential over-fitting induced by the noise in the CT measurements. Eq. 6 thus becomes

$$\begin{aligned} \theta^* &= \arg \min_{\theta} \left\{ \|\mathbf{y} - \mathbf{A}\hat{\mathbf{x}}\|_1 + \nabla(\hat{\mathbf{x}}) \right\}, \\ \nabla(\hat{\mathbf{x}}) &= \frac{1}{NM} \left( \sum_{i=1}^N \sum_{j=1}^{M-1} \|\hat{\mathbf{x}}_{i,j+1} - \hat{\mathbf{x}}_{i,j}\|_1 \right. \\ &\quad \left. + \sum_{i=1}^{N-1} \sum_{j=1}^M \|\hat{\mathbf{x}}_{i+1,j} - \hat{\mathbf{x}}_{i,j}\|_1 \right), \end{aligned} \quad (7)$$

where  $\hat{\mathbf{x}} \in \mathbb{R}^{N \times M}$ . Eq. 7 can be solved by NN training, and we can derive  $\mathbf{x}^*$  with the forward propagation of  $\mathcal{N}\mathcal{N}$  by

$$\mathbf{x}^* = \mathcal{N}\mathcal{N}(\mathbf{x}_{fbp}; \theta^*). \quad (8)$$

## 2.2. Solving the MAP

The proposed method can be considered as a kind of NN training-based reconstruction method, which optimizes the NN's parameters by minimizing the loss from both sinogram domain and image domain. The proposed LDCT reconstruction method can be divided into two steps: (1) Reconstructing the initial CT image: The initial CT image

is reconstructed using the FBP method. Although this initial CT image may contain many artifacts due to the low intensity of X-ray, FBP provides fundamental information about the internal structure of the human body, which is helpful for enhancing the reliability of the inversion result by NN. Moreover, FBP performs much faster than iterative reconstruction approaches such as compressive sensing; (2) Post-processing the initial reconstruction result: Once the initial CT image is achieved, it will be fed into a pre-defined NN and will be improved through the NN training. To achieve  $\theta^*$ , we establish the loss function for NN training based on Eq. 7,

$$\mathcal{L}(\mathbf{y}) = \frac{1}{NM} \|\mathbf{y} - \mathbf{A}\mathcal{N}\mathcal{N}(\mathbf{x}_{fbp}; \theta)\|_1 + \nabla(\mathcal{N}\mathcal{N}(\mathbf{x}_{fbp}; \theta)), \quad (9)$$

and we use gradient descent-based optimization algorithms such as stochastic gradient descent to optimize  $\theta$  to minimize the loss function. It is worth noting that the proposed method does not require setting weights for both the data fidelity term and the regularization term, which significantly reduces the difficulty of manually setting the weights. In summary, the visual flowchart of the iterative reconstruction for LDCT is shown in Fig. 1. Algorithm 1 further explains the construction algorithm in detail.

---

### Algorithm 1 Iterative reconstruction for LDCT imaging

**Require:** number of iterations:  $n$ ; CT measurements:  $\mathbf{y}$ ; FBP operator:  $\mathcal{F}$ ; projection matrix:  $\mathbf{A}$ ; learning rate:  $\lambda$   
**Ensure:** optimal  $\theta^*$

```

initial  $i = 1$ , initial CT image  $\mathbf{x}_0 = \mathcal{F}(\mathbf{y})$ 
while  $i <= n$  do
    reconstruct the CT image  $\mathcal{N}\mathcal{N}(\mathbf{x}_0; \theta)$ 
    compute the loss  $\mathcal{L}(\mathbf{y}) = \frac{1}{NM} \|\mathbf{y} - \mathbf{A}\mathcal{N}\mathcal{N}(\mathbf{x}_0; \theta)\|_1 + \nabla(\mathcal{N}\mathcal{N}(\mathbf{x}_0; \theta))$ 
    update  $\theta^* \leftarrow \theta - \lambda \frac{\partial \mathcal{L}}{\partial \theta}$ 
     $i \leftarrow i + 1$ 
return  $\mathbf{x}^* = \mathcal{N}\mathcal{N}(\mathbf{x}_0; \theta^*)$ 

```

---

## 2.3. NN Architecture

To enhance the quality of the initial CT image, we have designed a DNN with a straightforward structure. As depicted in Fig. 1, the network primarily consists of 2-D convolution, batch normalization, and LeakyReLU layers. The first layer is a convolution layer, followed by a LeakyReLU layer and a block composed of convolution, batch normalization (BN), and LeakyReLU. The convolution layers are employed for feature extraction, the BN layers for enhancing the stability of network training, and the LeakyReLU layers to ensure non-linearity throughout the network. LeakyReLU is defined as,

$$\text{LeakyReLU}(x) = \max(0, x) + \phi * \min(0, x). \quad (10)$$

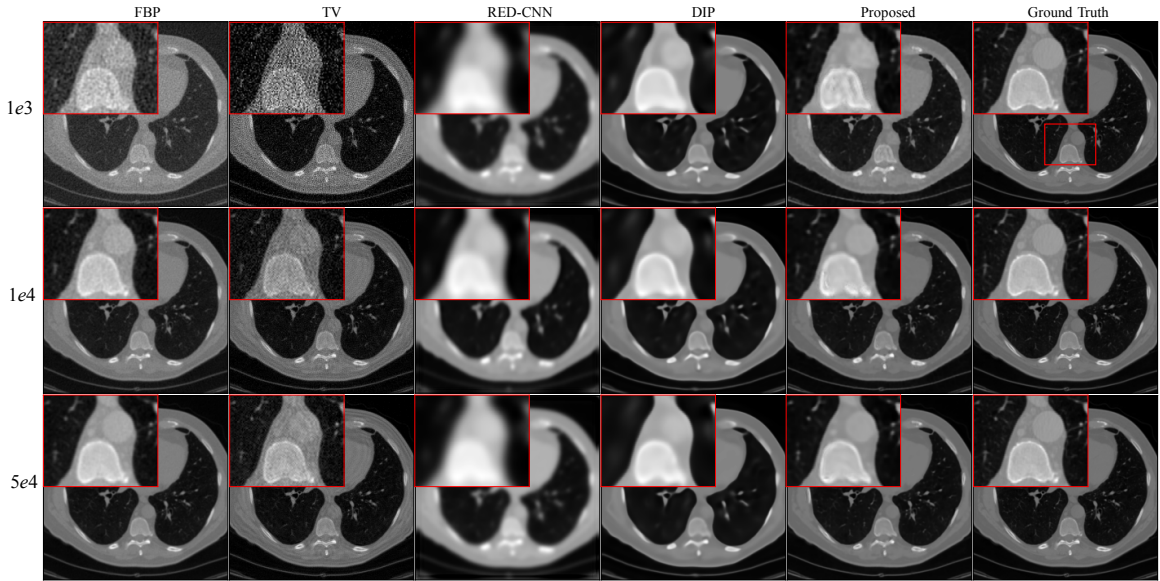


**Figure 5:** Reconstruction results of LoDoPab-CT data at different dose levels by different methods. Zoomed ROI images from the ground-truth image.

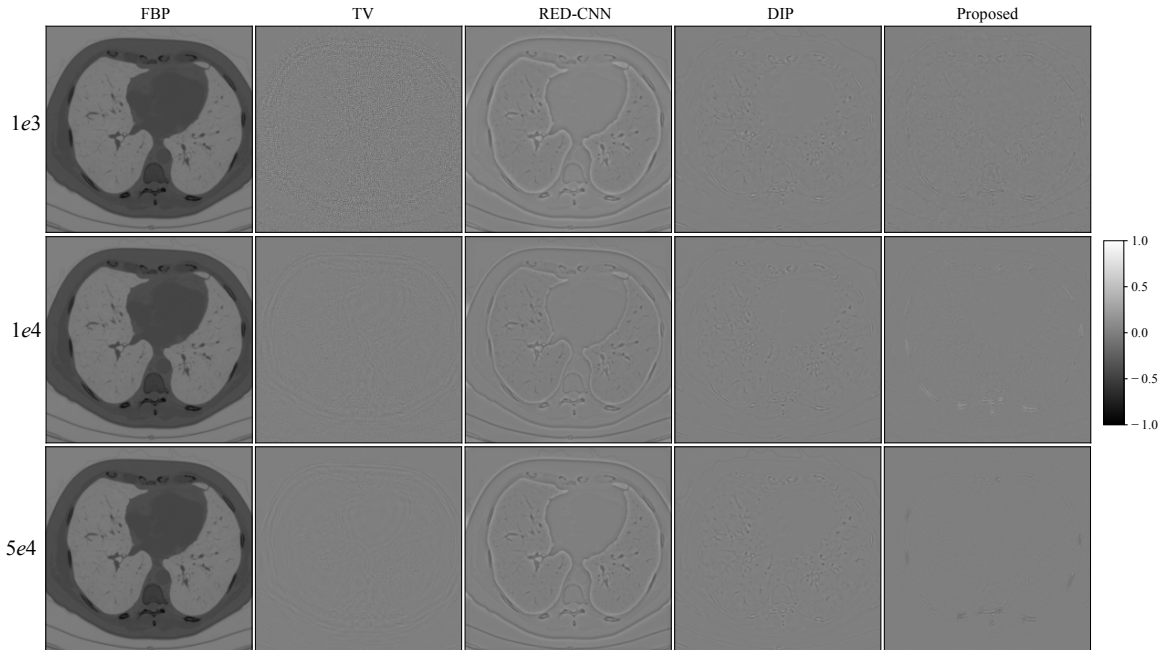


**Figure 6:** Reconstruction errors of LoDoPab-CT data at different dose levels by different methods.

In the subsequent experimental test, we set the value of  $\phi$  to 0.01.

### 3. Experimental Results

In this section, we evaluate the performance of the proposed method by comparing it with four representative methods: FBP, TV (post-processing and unsupervised method), DIP (unsupervised and data-free method), and RED-CNN (post-processing and supervised model).

#### 3.1. Parameter Setting

The FBP, TV and DIP reconstruction are implemented by using Deep Inversion Validation Library (<https://github.com/jleuschner/dival>) and Operator Discretization Library (<https://github.com/odlgroup/odl>). For TV and DIP reconstruction, we use the parameters recommend by Baguer, Leuschner and Schmidt (2020) (<https://github.com/otterobaguer/dip-ct-benchmark>). The NN training related tasks are all implemented on the PyTorch platform Paszke, Gross, Massa, Lerer, Bradbury, Chanan, Killeen, Lin, Gimelshein,

Antiga, Desmaison, Kopf, Yang, DeVito, Raison, Tejani, Chilamkurthy, Steiner, Fang, Bai and Chintala (2019).

For TV reconstruction, the weight for  $\ell_1$ -norm term is set to  $2.15 \times 10^{-7}$ , and the number of iterations is set to 200. For DIP reconstruction, we use a learning rate of 0.0005, 6 scales, 1000 iterations for AAPM challenge data and 2000 iterations for LoDoPaB-CT data, and 128 channels for the U-Net at every scale. We adopt mean square error (MSE) as the loss function for both TV and DIP reconstruction. In the proposed method, we set the iterations to 2000, and save the result with the highest peak signal-to-noise ratio (PSNR). For all reconstruction methods, the filter and frequency scaling of FBP reconstruction are set to Hann and 0.8, respectively.

For RED-CNN training, we use the AAPM Challenge Data as the training dataset. We train the RED-CNN using full-dose CT scans from nine patients, reserving one patient (L067) for evaluation. In the training data generation process, we use a patch size of 64. The batch size for RED-CNN training is set to 32, the number of training epochs is 100, the loss function is MSE loss, and we use Adam optimizer with a learning rate of  $10^{-5}$ . We train three models for different low-dose levels by using pairs of FBP reconstructions of low-dose simulations and corresponding full-dose CT images.

There are 30 convolution layers in our NN, the size of filter kernels of the first convolution layer is  $64 \times 1 \times 3 \times 3$ , where the format is number of filters  $\times$  number of channels  $\times$  width  $\times$  height. From the second to the penultimate convolution layer, we set the size of all filter kernels to  $64 \times 64 \times 3 \times 3$ . For the last convolution layer, the size of filter kernels is set to  $1 \times 64 \times 3 \times 3$ . We minimize the loss defined by Eq. 7 by using the AdamW method with learning rate of  $10^{-3}$ .

### 3.2. Data Specification

To evaluate the effectiveness of the proposed method, we test its performance on two datasets: AAPM challenge data and LoDoPaB-CT data Leuschner et al. (2021a). The AAPM challenge data consists of reconstructed simulated data from human abdomen CT scans provided by Mayo Clinic for the AAPM Low Dose CT Grand Challenge (<https://www.aapm.org/GrandChallenge/LowDoseCT/>). We use 1-mm slice thickness reconstructions with dimensions of 512 px  $\times$  512 px for RED-CNN training and performance comparison. The CT images from LoDoPaB-CT data are sampled from AAPM challenge data and have been cropped to dimensions of 362 px  $\times$  362 px. Additionally, these images have been subjected to dequantization noise uniformly distributed in  $[0,1]$  for each pixel.

For sinogram data simulation, we construct a 2-D fan-beam geometry with 1000 angles, 1000 pixels, source to axis distance 500 mm, and axis to detector distance 500 mm He, Zhang, Guan, Guan, Niu, Zhang, Chen and Liu (2022). The LDCT image are simulated by adding Poisson noise with  $I_i = [1e3, 1e4, 5e4]$  following the Poisson distribution according to the process of photon generation, attenuation, and detection, which can be expressed as,

$$y_i \sim \text{Poisson} \{ I_i e^{-[\mathbf{Ax}]_i} + \sigma_i \}, i = 1, \dots, m, \quad (11)$$

where  $I_i$  denotes the source intensity of the  $i$ -th X-ray,  $y_i$  represents the CT measurements produced by the  $i$ -th X-ray,  $\mathbf{A}$  is the projection matrix of CT imaging,  $\sigma_i$  denotes the background contributions of scatter and electrical noise, and  $\mathbf{x}$  represents the full-dose CT image. Additionally, the full-dose CT images  $\mathbf{x}$  are normalized before sinogram simulation by

$$x = \frac{x - \min(x)}{\max(x) - \min(x)}. \quad (12)$$

### 3.3. Quantitative Indices

We adopt two quantitative indices, PSNR and structural similarity index (SSIM), to quantify the quality of the reconstructed CT images. The PSNR expresses the ratio between the maximum possible power of a signal and the power of corrupting noise, which is measured by the mean squared error (MSE),

$$\begin{aligned} \text{PSNR}(\tilde{x}, x) &= 10 \log_{10} \left( \frac{\max(x)^2}{\text{MSE}(\tilde{x}, x)} \right), \\ \text{MSE}(\tilde{x}, x) &= \frac{1}{n} \sum_{i=1}^n |\tilde{x}_i - x_i|^2, \end{aligned} \quad (13)$$

where  $x$  and  $\tilde{x}$  denotes the ground truth image and the reconstruction, respectively, and  $n$  is the number of pixels in the reconstructed image. A higher PSNR value indicates better reconstruction quality.

The SSIM, which lies in the range  $[0, 1]$ , is used to measure the similarity between the ground-truth image and the reconstruction image,

$$\text{SSIM}(\tilde{x}, x) = \frac{1}{M} \sum_{j=1}^M \frac{(2\tilde{\mu}_j \mu_j + C_1)(2\Sigma_j + C_2)}{(\tilde{\mu}_j^2 + \mu_j^2 + C_1)(\tilde{\sigma}_j^2 + \sigma_j^2 + C_2)}, \quad (14)$$

where  $\tilde{\mu}_j$  and  $\mu_j$  are the average pixel intensities,  $\tilde{\sigma}_j^2$  and  $\sigma_j^2$  represent the variances, and  $\Sigma_j$  is the covariance of  $\tilde{x}, x$  at the  $j$ -th local window. The constants  $2C_1 = (K_1 L)^2$  and  $C_2 = (K_2 L)^2$  tend to be zero to avoid instability. Following Wang, Bovik, Sheikh and Simoncelli (2004) and Leuschner, Schmidt, Ganguly, Andriashen, Coban, Denker, Bauer, Hadjifaradji, Batenburg, Maass and van Eijnatten (2021b), we choose  $K_1 = 0.01$ ,  $K_2 = 0.03$ ,  $L = \max(x) - \min(x)$ , and the window size is  $7 \times 7$ . A higher SSIM value indicates better reconstruction quality.

### 3.4. Reconstruction Results

*AAPM challenge data:* We randomly select three full-dose CT images from AAPM challenge data to evaluate

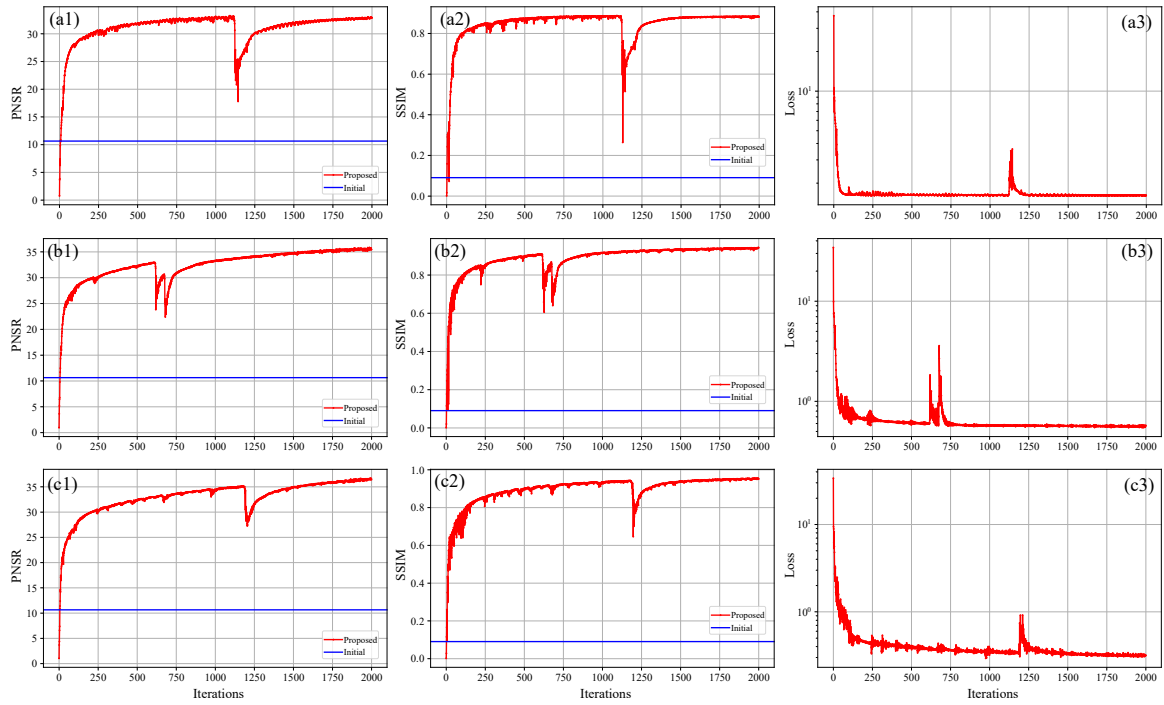


Figure 7: Convergence tendency of the proposed method in LoDoPab-CT data reconstruction

effectiveness of the propose method with the X-ray source intensity  $I_i = [1e3, 1e4, 5e4]$ . From Fig. 2, Fig. 3 and Fig. 4, we can observe that the quality of the FBP reconstruction images degraded significant as the X-ray source intensity decreased, resulting in amplified noise and artifacts distributed throughout the entire image. As a post-processing method, TV achieves higher quality images by post-processing the reconstructed images through FBP. Another post-processing and supervised method RED-CNN, can effectively remove noise and artifacts, but it tends to smooth out some tiny structures. Although DIP is unsupervised and takes random noise as input, it can effectively remove noise while producing images with higher resolution than RED-CNN. Comparing the reconstructed results by different methods, we can see that the proposed method achieves the best performance in terms of noise and artifacts attenuation and preservation of tiny structures.

To better illustrate the effectiveness of the proposed method, we further demonstrate the zoomed-in results corresponding to the red box in each ground truth. As shown in Fig. 2, Fig. 3 and Fig. 4, the reconstructed results by FBP and TV are contaminated by noise and artifacts. Although RED-CNN and DIP can suppress the noise, many valuable details are smoothed out. In comparison, the proposed method achieves better reconstruction accuracy than the competitive methods. It is worth noting that although the ground-truth images are norm-dose CT images, slight noise and artifacts still remain in them. Furthermore, the reconstructed results by the proposed method outperform the ground-truth images in terms of resolution, particularly with  $I_i = 1e4$  and  $5e4$ .

*LoDoPab-CT data:* For the LoDoPab-CT data, the reconstruction results are shown in Fig. 5. From Fig. 5, we

can observe that the performance of each reconstruction method is similar to their performance for the above AAPM challenge data reconstruction. The reconstructed results by FBP and TV suffer from noise and artifacts, although TV can suppress a lot of noise. The textures and edges in the reconstructed results by RED-CNN are smoothed out, whereas DIP can remove noise and preserve tiny structures more effectively. The proposed method achieves the best performance with regard to noise suppression and preservation of tiny structures. Furthermore, the reconstruction errors (Fig. 6) further demonstrate that FBP method sacrifices a lot of useful information. TV and RED-CNN can effectively improve the reconstructed results by FBP; however, TV can not preserver edges well, and RED-CNN tends to smooth edges and textures. DIP has slighter residual errors in terms of edges and textures. Compared with the competitive methods, the proposed method significantly decreases the reconstruction errors by FBP and achieves minimal reconstruction errors.

To quantitatively analyze the performance of our method, we calculate the the PSNR and SSIM values of the above reconstruction results, including the AAPM challenge data and the LoDoPab-CT data. As shown in Table. 1, our method achieves the highest PSNR and SSIM among the five approaches, except for the reconstruction task of AAPM-2 with respect of the SSIM under  $I_i = 1e3$  and of AAPM-3 with respect of the PSNR under  $I_i = 1e3$ . Specifically, the SSIM and PSNR of DIP are 0.06 and 0.24 dB higher than those of the proposed method.

In addition, we take the evolution curves of PSNR and SSIM versus iteration of LoDoPab-CT data reconstruction as an example to illustrate the convergence of the proposed

**Table 1**

Quantitative Results (PSNR/SSIM) of Different Algorithms for three cases of AAPM data reconstruction.

Data	$I_i$	FBP	TV	RED-CNN	DIP	Proposed
AAPM-1	1e3	10.92/0.09	14.51/0.19	23.54/0.64	29.83/0.81	<b>32.37/0.82</b>
	1e4	10.92/0.09	21.19/0.37	25.39/0.74	30.22/0.82	<b>35.99/0.92</b>
	5e4	10.92/0.09	26.25/0.54	24.23/0.69	30.36/0.82	<b>37.85/0.94</b>
AAPM-2	1e3	9.75/0.12	12.86/0.16	24.89/0.68	31.46/ <b>0.85</b>	<b>31.56/0.79</b>
	1e4	9.75/0.12	19.32/0.31	27.49/0.79	30.33/0.83	<b>35.30/0.92</b>
	5e4	9.75/0.12	25.21/0.49	25.89/0.75	31.94/0.85	<b>38.06/0.94</b>
AAPM-3	1e3	10.89/0.13	13.30/0.17	25.71/0.73	<b>35.71/0.90</b>	<b>35.47/0.90</b>
	1e4	10.89/0.13	19.99/0.30	28.35/0.83	36.24/0.91	<b>38.07/0.93</b>
	5e4	10.89/0.13	26.03/0.47	26.64/0.80	35.20/0.90	<b>37.72/0.94</b>
LoDoPab-CT	1e3	10.65/0.09	15.72/0.22	24.33/0.65	32.76/0.88	<b>33.25/0.89</b>
	1e4	10.65/0.09	24.26/0.45	26.12/0.73	33.14/0.88	<b>35.84/0.94</b>
	5e4	10.65/0.09	29.24/0.65	24.95/0.70	32.82/0.87	<b>36.39/0.95</b>

**Table 2**

Computation Time of Different Algorithms for LoDoPab-CT Data Reconstruction.

Method	GPU time	
	Training	Reconstruction
FBP (s)	/	0.1
TV (s/iteration)	/	0.07
RED-CNN (s/epoch)	310	5.1
DIP (s/iteration)	/	3.11
Proposed (s/iteration)	/	1.02

method. As shown in Fig. 7, the PSNR and SSIM increase while the loss decreases rapidly, which reveals that the proposed method can converge quickly. Specifically, the curves of PSNR and SSIM begin to converge after about 250 iterations, and the curves of loss start to converge after about 100 iterations. Although there are some fluctuations in these curves since the measurements contain noise, they converge quickly again, which indicates the good robustness of our method. Table 2 lists the computation time of different method on a single GPU (Nvidia Tesla K80), it can be seen that FBP, TV and the proposed method have great disadvantages in terms of reconstruction time. Although RED-CNN only need one inference to reconstruct the high-quality image, the process of NN training is time consuming.

#### 4. Discussion and Conclusion

For the initial LDCT reconstruction, we utilize the results reconstructed by FBP as the initial model for the proposed method. FBP can extract fundamental information

about the internal structure of the human body, despite potential contamination from artifacts caused by the low intensity of X-ray. This is crucial for neural network-based LDCT imaging, as the black-box nature of these networks can significantly decrease the reliability of LDCT reconstruction results. It's also important to note that the quality of the initial reconstructed image can impact the performance of the proposed method. One could substitute the FBP input with a high-quality image to further improve resolution. Additionally, FBP often performs much faster than iterative reconstruction approaches such as compressive sensing, which aids in enhancing inversion efficiency. Although our proposed method can converge rapidly, fluctuations due to noise in measurements might negatively impact the reconstruction efficiency. In future work, we aim to investigate better regularization techniques to promote convergence stability.

In this work, we propose an unsupervised and training data-free method for LDCT imaging. The proposed method aims to improve the initial reconstruction results with low quality, which reconstructs the high-quality image by DNN training without any training samples. We implement the DNN training by minimizing the  $\ell_1$ -norm distance between the CT measurements and their corresponding simulated sinogram data on the reconstructed image and the TV value of the reconstructed image. Notably, the proposed method dose not need to set weights for both the data fidelity term and the regularization term, which significantly reduces the difficulty of manually setting the weights. Experimental results on the AAPM challenge data and LoDoPab-CT data demonstrate that the proposed method could achieve better performance than the representative non-learning methods and supervised method, with higher resolution and lower computational cost. The proposed method can be implemented flexible and has the

potential to be applied to other medical image reconstruction problems, including sparse-view CT reconstruction and image reconstruction from sparse samples in MRI. These applications are particularly useful when collecting training samples is either expensive or difficult.

## Acknowledgment

This work was supported in part by the National Natural Science Foundation of China under Grant 41774079 and Grant 61906170, and in part by the Project of the Science and Technology Plan for Zhejiang Province (No.LGF21F020023), and in part by the Plan Project of Ningbo Municipal Science and Technology (Nos.2022Z233, 2021Z050, 2022S002 and 2023J403).

## CRedit authorship contribution statement

**Feng Wang:** Conceptualization, Investigation, Software, Validation, Methodology, Writing review & editing.. **Renfang Wang:** Conceptualization, Methodology, Software, Supervision, Writing review & editing. **Bo Yang:** Investigation, Methodology, Software, Validation, Visualization, Writing review & editing. **Hong Qiu:** Investigation, Methodology, Software, Validation, Writing review & editing.

## Declaration of competing interest

The authors declare that they have no known competing financial interests or personal relationships that could have appeared to influence the work reported in this paper

## References

- Baguer, D.O., Leuschner, J., Schmidt, M., 2020. Computed tomography reconstruction using deep image prior and learned reconstruction methods. *Inverse Problems* 36, 094004. URL: <https://dx.doi.org/10.1088/1361-6420/aba415>, doi:10.1088/1361-6420/aba415. publisher: IOP Publishing.
- Batson, J., Royer, L., 2019. Noise2Self: Blind Denoising by Self-Supervision. URL: <http://arxiv.org/abs/1901.11365>, doi:10.48550/arXiv.1901.11365 [cs, stat].
- Cai, J.F., Jia, X., Gao, H., Jiang, S.B., Shen, Z., Zhao, H., 2014. Cine Cone Beam CT Reconstruction Using Low-Rank Matrix Factorization: Algorithm and a Proof-of-Principle Study. *IEEE Trans. Med. Imaging* 33, 1581–1591. URL: <https://ieeexplore.ieee.org/document/6803058/>, doi:10.1109/TMI.2014.2319055.
- Chen, H., Zhang, Y., Kalra, M.K., Lin, F., Chen, Y., Liao, P., Zhou, J., Wang, G., 2017. Low-Dose CT With a Residual Encoder-Decoder Convolutional Neural Network. *IEEE Transactions on Medical Imaging* 36, 2524–2535. doi:10.1109/TMI.2017.2715284. conference Name: IEEE Transactions on Medical Imaging.
- Cheng, W., Wang, Y., Li, H., Duan, Y., 2020. Learned Full-Sampling Reconstruction From Incomplete Data. *IEEE Transactions on Computational Imaging* 6, 945–957. doi:10.1109/TCI.2020.2996751. conference Name: IEEE Transactions on Computational Imaging.
- Ding, Q., Ji, H., Quan, Y., Zhang, X., 2022. A dataset-free deep learning method for low-dose CT image reconstruction. *Inverse Problems* 38, 104003. URL: <https://dx.doi.org/10.1088/1361-6420/ac8ac6>, doi:10.1088/1361-6420/ac8ac6. publisher: IOP Publishing.
- Gong, K., Catana, C., Qi, J., Li, Q., 2019. PET Image Reconstruction Using Deep Image Prior. *IEEE Trans. Med. Imaging* 38, 1655–1665. URL: <https://ieeexplore.ieee.org/document/8581448/>, doi:10.1109/TMI.2018.2888491.
- Hasan, A.M., Mohebbian, M.R., Wahid, K.A., Babyn, P., 2021. Hybrid-Collaborative Noise2Noise Denoiser for Low-Dose CT Images. *IEEE Transactions on Radiation and Plasma Medical Sciences* 5, 235–244. doi:10.1109/TRPMS.2020.3002178. conference Name: IEEE Transactions on Radiation and Plasma Medical Sciences.
- He, Z., Zhang, Y., Guan, Y., Guan, B., Niu, S., Zhang, Y., Chen, Y., Liu, Q., 2022. Iterative Reconstruction for Low-Dose CT Using Deep Gradient Priors of Generative Model. *IEEE Transactions on Radiation and Plasma Medical Sciences* 6, 741–754. doi:10.1109/TRPMS.2022.3148373. conference Name: IEEE Transactions on Radiation and Plasma Medical Sciences.
- Hendriksen, A.A., Pelt, D.M., Batenburg, K.J., 2020. Noise2Inverse: Self-supervised deep convolutional denoising for tomography. *IEEE Trans. Comput. Imaging* 6, 1320–1335. URL: <http://arxiv.org/abs/2001.11801>, doi:10.1109/TCI.2020.3019647. arXiv:2001.11801 [cs, eess, stat].
- Jin, K.H., McCann, M.T., Froustey, E., Unser, M., 2017. Deep Convolutional Neural Network for Inverse Problems in Imaging. *IEEE Transactions on Image Processing* 26, 4509–4522. doi:10.1109/TIP.2017.2713099. conference Name: IEEE Transactions on Image Processing.
- Kandarpa, V.S.S., Bousse, A., Benoit, D., Visvikis, D., 2021. DUG-RECON: A Framework for Direct Image Reconstruction Using Convolutional Generative Networks. *IEEE Transactions on Radiation and Plasma Medical Sciences* 5, 44–53. doi:10.1109/TRPMS.2020.3033172. conference Name: IEEE Transactions on Radiation and Plasma Medical Sciences.
- Kang, E., Min, J., Ye, J.C., 2017. A deep convolutional neural network using directional wavelets for low-dose X-ray CT reconstruction. *Med Phys* 44, e360–e375. doi:10.1002/mp.12344.
- Kim, K., Ye, J.C., Worstell, W., Ouyang, J., Rakvongthai, Y., Fakhri, G.E., Li, Q., 2015. Sparse-View Spectral CT Reconstruction Using Spectral Patch-Based Low-Rank Penalty. *IEEE Trans. Med. Imaging* 34, 748–760. URL: <https://ieeexplore.ieee.org/document/6985637/>, doi:10.1109/TMI.2014.2380993.
- Lehtinen, J., Munkberg, J., Hasselgren, J., Laine, S., Karras, T., Aittala, M., Aila, T., 2018. Noise2Noise: Learning Image Restoration without Clean Data. URL: <http://arxiv.org/abs/1803.04189>, doi:10.48550/arXiv.1803.04189, arXiv:1803.04189 [cs, stat].
- Leuschner, J., Schmidt, M., Baguer, D.O., Maass, P., 2021a. LoDoPaB-CT, a benchmark dataset for low-dose computed tomography reconstruction. *Sci Data* 8, 109. URL: <https://www.nature.com/articles/s41597-021-00893-z>, doi:10.1038/s41597-021-00893-z. number: 1 Publisher: Nature Publishing Group.
- Leuschner, J., Schmidt, M., Ganguly, P.S., Andriashen, V., Coban, S.B., Denker, A., Bauer, D., Hadjifaradji, A., Batenburg, K.J., Maass, P., van Eijnen, M., 2021b. Quantitative Comparison of Deep Learning-Based Image Reconstruction Methods for Low-Dose and Sparse-Angle CT Applications. *Journal of Imaging* 7, 44. URL: <https://www.mdpi.com/2313-433X/7/3/44>, doi:10.3390/jimaging7030044. number: 3 Publisher: Multidisciplinary Digital Publishing Institute.
- Liu, J., Li, J., 2020. Sparse-sampling CT Sinogram Completion using Generative Adversarial Networks, in: 2020 13th International Congress on Image and Signal Processing, BioMedical Engineering and Informatics (CISP-BMEI), IEEE, Chengdu, China. pp. 640–644. URL: <https://ieeexplore.ieee.org/document/9263571/>, doi:10.1109/CISP-BMEI51763.2020.9263571.
- Ma, J., Zhang, H., Gao, Y., Huang, J., Liang, Z., Feng, Q., Chen, W., 2012. Iterative image reconstruction for cerebral perfusion CT using a pre-contrast scan induced edge-preserving prior. *Phys. Med. Biol.* 57, 7519–7542. URL: <https://iopscience.iop.org/article/10.1088/0031-9155/57/22/7519>, doi:10.1088/0031-9155/57/22/7519.
- Paszke, A., Gross, S., Massa, F., Lerer, A., Bradbury, J., Chanan, G., Killeen, T., Lin, Z., Gimelshein, N., Antiga, L., Desmaison, A., Kopf, A., Yang, E., DeVito, Z., Raison, M., Tejani, A., Chilamkurthy, S., Steiner, B., Fang, L., Bai, J., Chintala, S., 2019. PyTorch: An Imperative Style, High-Performance Deep Learning Library, in: Advances in Neural Information Processing Systems 32. Curran Associates,

Inc., pp. 8024–8035. URL: <http://papers.neurips.cc/paper/9015-pytorch-an-imperative-style-high-performance-deep-learning-library.pdf>.

Qiong Xu, Hengyong Yu, Xuanqin Mou, Lei Zhang, Jiang Hsieh, Ge Wang, 2012. Low-Dose X-ray CT Reconstruction via Dictionary Learning. *IEEE Trans. Med. Imaging* 31, 1682–1697. URL: <http://ieeexplore.ieee.org/document/6188527/>, doi:10.1109/TMI.2012.2195669.

Sidky, E.Y., Pan, X., 2008. Image reconstruction in circular cone-beam computed tomography by constrained, total-variation minimization. *Phys Med Biol* 53, 4777–4807. doi:10.1088/0031-9155/53/17/021.

Smith-Bindman, R., Lipson, J., Marcus, R., Kim, K.P., Mahesh, M., Gould, R., Berrington de González, A., Miglioretti, D.L., 2009. Radiation dose associated with common computed tomography examinations and the associated lifetime attributable risk of cancer. *Arch Intern Med* 169, 2078–2086. doi:10.1001/archinternmed.2009.427.

Ulyanov, D., Vedaldi, A., Lempitsky, V., 2020. Deep Image Prior. *Int J Comput Vis* 128, 1867–1888. URL: <http://arxiv.org/abs/1711.10925>, doi:10.1007/s11263-020-01303-4. arXiv:1711.10925 [cs, stat].

Wang, Z., Bovik, A., Sheikh, H., Simoncelli, E., 2004. Image Quality Assessment: From Error Visibility to Structural Similarity. *IEEE Trans. on Image Process.* 13, 600–612. URL: <http://ieeexplore.ieee.org/document/1284395/>, doi:10.1109/TIP.2003.819861.

Wu, D., Kim, K., Li, Q., 2019. Computationally efficient deep neural network for computed tomography image reconstruction. *Med Phys* 46, 4763–4776. doi:10.1002/mp.13627.

Yokota, T., Kawai, K., Sakata, M., Kimura, Y., Hontani, H., 2019. Dynamic PET Image Reconstruction Using Nonnegative Matrix Factorization Incorporated With Deep Image Prior, in: 2019 IEEE/CVF International Conference on Computer Vision (ICCV), pp. 3126–3135. doi:10.1109/ICCV.2019.890622. iSSN: 2380-7504.

Yoo, J., Jin, K.H., Gupta, H., Yerly, J., Stuber, M., Unser, M., 2021. Time-Dependent Deep Image Prior for Dynamic MRI. *IEEE Trans. Med. Imaging* 40, 3337–3348. URL: <https://ieeexplore.ieee.org/document/9442767/>, doi:10.1109/TMI.2021.3084288.

Yuan, N., Zhou, J., Gong, K., Qi, J., 2019. Low-dose CT count-domain denoising via convolutional neural network with filter loss, in: Bosmans, H., Chen, G.H., Gilat Schmidt, T. (Eds.), *Medical Imaging 2019: Physics of Medical Imaging*, SPIE, San Diego, United States. p. 26. URL: <https://www.spiedigitallibrary.org/conference-proceedings-of-spie/10948/2513479/Low-dose-CT-count-domain-denoising-via-convolutional-neural-network/10.1117/12.2513479.full>, doi:10.1117/12.2513479.

Yuan, N., Zhou, J., Qi, J., 2020. Half2Half: deep neural network based CT image denoising without independent reference data. *Phys. Med. Biol.* 65, 215020. URL: <https://dx.doi.org/10.1088/1361-6560/aba939>, doi:10.1088/1361-6560/aba939. publisher: IOP Publishing.

Zhang, Y., Xi, Y., Yang, Q., Cong, W., Zhou, J., Wang, G., 2016. Spectral CT Reconstruction With Image Sparsity and Spectral Mean. *IEEE Trans. Comput. Imaging* 2, 510–523. URL: <http://ieeexplore.ieee.org/document/7567594/>, doi:10.1109/TCI.2016.2609414.

Zheng, A., Gao, H., Zhang, L., Xing, Y., 2020. A dual-domain deep learning-based reconstruction method for fully 3D sparse data helical CT. *Phys Med Biol* 65, 245030. doi:10.1088/1361-6560/ab8fc1.

Zhu, B., Liu, J.Z., Cauley, S.F., Rosen, B.R., Rosen, M.S., 2018. Image reconstruction by domain-transform manifold learning. *Nature* 555, 487–492. URL: <https://www.nature.com/articles/nature25988>, doi:10.1038/nature25988. number: 7697 Publisher: Nature Publishing Group.